European Journal of Chemistry

View Journal Online
View Article Online

Synthesis and properties of photocatalysts for the high degradation of sulfadiazine

Zhenzhao Pei * and Feng Li

Department of Chemical Engineering, School of Materials Science and Engineering, Hebei University of Engineering, Handan 056038, P.R. China
peizhenzhaophd@126.com (Z.P.), 17862002202@163.com (F.L.)

* *Corresponding author at: Department of Chemical Engineering, School of Materials Science and Engineering, Hebei University of Engineering, Handan 056038, P.R. China.*
e-mail: peizhenzhaophd@126.com (Z. Pei).

RESEARCH ARTICLE

10.5155/eurjchem.12.2.117-123.2079

Received: 23 January 2021
Received in revised form: 09 April 2021
Accepted: 17 April 21
Published online: 30 June 2021
Printed: 30 June 2021

KEYWORDS

Sulfadiazine
Degradation
Sulfonamides
Photocatalysis
BiOBr/Bi3.84W0.16O6.24
Simulated solar light irradiation

ABSTRACT

In this study, it was discovered for the first time that the BiOBr/$Bi_{3.84}W_{0.16}O_{6.24}$ catalyst can efficiently degrade sulfadiazine (SDZ). Multiple techniques, such as X-ray diffraction (XRD), scanning electron microscopy (SEM), and UV-Vis diffuse reflection spectroscopy (DRS) were applied to research the structures, morphology and photocatalytic properties of as-prepared samples. In addition, the effect of different synthesis pH environment and initial SDZ solution pH on the catalyst degradation efficiency were discussed. The BiOBr/$Bi_{3.84}W_{0.16}O_{6.24}$ catalyst synthesized under the condition of pH = 7 exhibited excellent photocatalytic activity for photodegradation of SDZ of 91% within 120 min under simulated solar light irradiation. Also, the roles of the radical species have been studied, and the $\cdot O_2^-$ and h^+ were proved to dominate the photocatalytic process. Based on the experimental results, the photocatalytic mechanism was proposed.

Cite this: *Eur. J. Chem.* **2021**, *12(2)*, 117-123 **Journal website**: www.eurjchem.com

1. Introduction

With the gradual improvement of living standards and economic capacity, people's medical awareness also gradually improves. People use antibiotics more and more frequently in daily life, and their usage is also increasing. Antibiotics are mainly used in healthcare, animal husbandry, and aquaculture [1]. At the same time, antibiotics, as trace pollutants, are causing increasingly serious pollution to environmental water bodies [2]. Sulfadiazine (SDZ, $C_{10}H_{10}N_4O_2S$) belongs to the sulfa antibiotics and is one of the most commonly used human and veterinary antibiotics. It has been detected many times in the water source environment, which affects the growth of aquatic plants and harms human health [3].

Traditional industrial wastewater treatment methods are generally obtained through physical methods such as precipitation, filtration, adsorption, or chemical treatment methods that add chemical substances to convert them into other products through oxidation-reduction reactions and biodegradation methods. Although the above water treatment technologies are widely used in real life, they also have the limitations of incomplete removal, secondary pollution, or high cost and low efficiency [4]. Therefore, it has always been the goal that people pursue to find a green, efficient, and thoroughly degradable pollutant treatment method. Semiconductor photocatalysis technology is a kind of green technology that uses sunlight as a direct driving force and is recognized as the most promising green technology. The photocatalytic oxidation technology represented by semiconductor photocatalysts has attracted wide attention from researchers due to its low consumption, high stability, high efficiency, and environmental friendliness [5].

Bismuth-based semiconductor is a kind of advanced photocatalytic functional material with unique prospects developed in recent years. Its unique electronic structure provides a suitable band gap for visible light response and is a promising new type of visible light driven photocatalyst [6,7]. Among them, Bi_2WO_6 and BiOX (X = Cl, Br, I) have attracted the attention of a large number of scientific researchers. During the synthesis of Bi_2WO_6, a special $Bi_{3.84}W_{0.16}O_{6.24}$ crystal was discovered. As one of bismuth tungsten composite oxides, it has attracted enormous attention. Wang *et al.* [8] synthesized $Bi_{3.84}W_{0.16}O_{6.24}$ by hydrothermal method under pH = 1 and 2 and studied its ability to degrade bisphenol A (BPA) under simulated solar light irradiation.

ISSN 2153-2249 (Print) / ISSN 2153-2257 (Online)
https://dx.doi.org/10.5155/eurjchem.12.2.117-123.2079

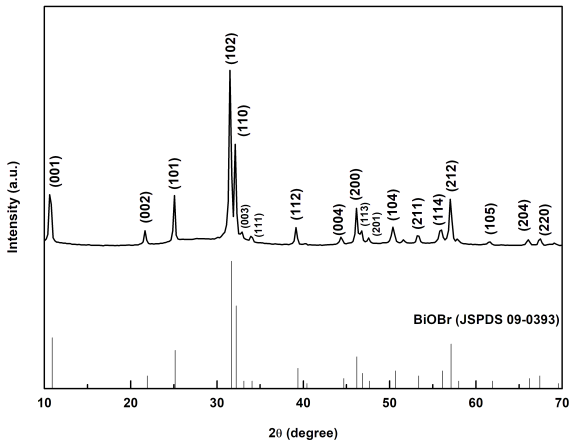

Figure 1. The XRD pattern of the as-prepared samples: synthesized without ammonia water.

Hou *et al.* [9] used different alkalis to adjust the pH of the reaction solution and successfully prepared $Bi_{3.84}W_{0.16}O_{6.24}$ photocatalysts with various microstructures, which have excellent degradation ability for methyl orange (MO). Li *et al.* [10] successfully prepared Ag / $Bi_{3.84}W_{0.16}O_{6.24}$ composite photocatalyst at room temperature by using silver nitrate ($AgNO_3$) as the silver source. The photocatalytic degradation of tetracycline (TC) was carried out under visible light to study the effect of Ag content.

In this study, we synthesized the BiOBr/$Bi_{3.84}W_{0.16}O_{6.24}$ material via a microwave method by adding ammonia water to the synthesis system. And found that it can be effectively used for the degradation of sulfadiazine. Compared with the pure BiOBr synthesized without ammonia water, the photocatalytic efficiency of the catalyst was doubled. So far, no one has reported in the literature. Furthermore, the photocatalytic mechanism for the degradation of SDZ was also analyzed.

2. Experimental

2.1. Materials

Bismuth nitrate pentahydrate ($Bi(NO_3)_3{\cdot}5H_2O$, ≥99.0%) and ethylene glycol (EG) were purchased from Tianjin Zhiyuan Chemical Reagent Co., Ltd. Potassium bromide (KBr, ≥99.0%) and $Na_2WO_4{\cdot}2H_2O$ were bought from Sinopharm Chemical Reagent Co., Ltd. Ammonia water was purchased from Tianjin Kaitong Chemical Reagent Co., Ltd. Sulfadiazine ($C_{10}H_{10}N_4O_2S$, SDZ, 98%) was obtained from Shanghai Aladdin Biochemical Technology Co., Ltd. Deionized water was obtained from laboratory water purification treatment equipment and used for all experimental work. All reagents in this work were employed without further purification.

2.2. Synthesis

The catalysts were synthesized through microwave method. Detailed steps are as follows, 1.4552 g $Bi(NO_3)_3{\cdot}5H_2O$ were dissolved in 20 mL deionized water containing 1 mL concentrated nitric acid. Meanwhile, 0.3299 g $Na_2WO_4{\cdot}2H_2O$ and 0.238 g KBr were dissolved in 20 mL ethylene glycol. The above two solutions were then mixed. Set the mixed solution to different synthesis conditions (no pH adjustment or adjusted the pH to 1, 3, 5, 7, and 9 by NH_4OH solution under continued stirring at room temperature). Subsequently, the mixed solution was put into a microwave reactor and heated for 30 minutes under a microwave power of 300 W, then allowed to cool to room temperature naturally. The resulting precipitates were collected and washed three times with deionized water and absolute ethanol, respectively, and dried at 80 °C.

2.3. Characterization

X-ray diffraction (XRD) patterns of all samples were identified by using a Bruker Automatic Diffractometer (Bruker D8 Advance) with CuKα radiation. UV/Vis diffuse reflectance spectroscopy (DRS) were obtained on an ultraviolet-visible spectrophotometer (TU-1901) with $BaSO_4$ was used as a reference. The morphology of the materials was analyzed by scanning electron microscopy (SEM, JSM6360LV).

2.4. Photocatalytic activity measurement

The photocatalytic performance of all samples was investigated by using SDZ as target pollutant under simulated solar light irradiation. A 300 W Xe lamp was used as the light source. In a typical photocatalytic experiment, 50 mg photocatalyst was dispersed in SDZ solution (100 mL, 10 mg/L) with continuous stirring. Prior to the irradiation, the mixed solution was magnetically stirred for 40 min in the dark to attain an adsorption-desorption equilibrium. During every irradiation time interval of 20 min, about 4 mL of solution was collected and centrifuged to remove the photocatalyst particles. The SDZ concentrations were analyzed with a UV-vis spectrophotometer (TU-1901) at the absorption wavelength 265 nm.

3. Results and discussion

3.1. XRD analysis

The crystal structures of the as-prepared photocatalysts were investigated by the XRD method, as shown in Figures 1 and 2. Figure 1 shows the XRD pattern of the sample prepared without ammonia water, while Figure 2 shows the XRD of the samples synthesized by using ammonia water to adjust the pH to 1, 3, 5, 7, and 9, respectively.

The result indicates that the diffraction peak of the sample synthesized without ammonia water is in good agreement with the tetragonal phase of BiOBr (JCPDS card no. 09-0393). No traces of each other were detected, indicating that the synthesized substance is pure BiOBr. This result proved that bismuth and tungsten cannot be combined without ammonia water.

When ammonia is added to adjust the pH value of the synthesis system to 1, 3, and 5, it can be clearly observed that the characteristic peak intensity of BiOBr gradually decreases or even disappears, and the characteristic peaks of other substances are not observed in Figure 2.

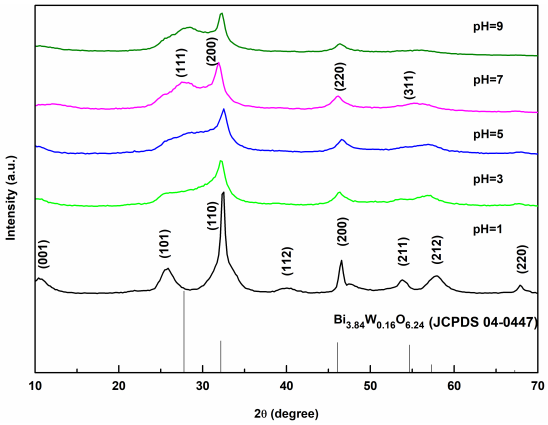

Figure 2. The XRD patterns of the as-prepared samples: adjust the pH of the system to different values with ammonia water.

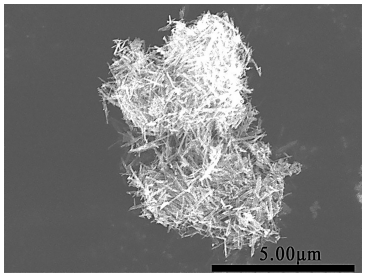

Figure 3. SEM image of the samples: synthesized without ammonia water.

When the pH value is further adjusted to 7, new diffraction peaks appear at 2 θ = 27.82, 31.96, 46.13 and 54.83 °, which are in good agreement with (111), (200), (220) and (311) crystal planes of standard card (JCPDS No.43-0447), indicating that it contains tungsten bismuth oxide $Bi_{3.84}W_{0.16}O_{6.24}$. At this time, the diffraction peak intensity of the (001) plane of BiOBr does not disappear completely, which indicates that there are two phases of BiOBr and $Bi_{3.84}W_{0.16}O_{6.24}$ in the sample. When the pH was adjusted to 9, the intensity of the characteristic diffraction peak of $Bi_{3.84}W_{0.16}O_{6.24}$ was lower than that of pH = 7, indicating that the synthesis of $Bi_{3.84}W_{0.16}O_{6.24}$ was inhibited when the pH was too high. In summary, as the amount of ammonia increased, the synthesis of BiOBr was inhibited and the content gradually decreased. The content of $Bi_{3.84}W_{0.16}O_{6.24}$ showed a trend of first increasing and then being inhibited.

The possible formation process of $Bi_{3.84}W_{0.16}O_{6.24}$ is as follows:

$$Bi(NO_3)_3 + H_2O \rightarrow BiONO_3 \downarrow + 2HNO_3 \quad (1)$$

$$Na_2WO_4 + 2H^+ \rightarrow H_2WO_4 \downarrow + 2Na^+ \quad (2)$$

$$Bi^{3+} + 3OH^- \rightarrow Bi(OH)_3 \downarrow \quad (3)$$

$$nBi^{3+} + 2nOH^- \rightarrow [BinOn]^{n+} + nH_2O \quad (4)$$

$$H^+ + OH^- \rightarrow H_2O \quad (5)$$

$$2Bi(OH)_3 + H_2WO_4 \rightarrow Bi_2WO_6 \downarrow + 4H_2O \quad (6)$$

$$2BiONO_3 + H_2WO_4 \rightarrow Bi_2WO_6 \downarrow + 2HNO_3 \quad (7)$$

$Bi(NO_3)_3$ is hydrolyzed into $BiONO_3$ precipitate in water, and Na_2WO_4 is hydrolyzed into H_2WO_4 in acid condition. When ammonia is not added into the system, the measured pH is less than 1, and the solution is strongly acidic at this time. In a strong acid solution, the H_2WO_4 colloid is positively charged and repulses with a small amount of Bi^{3+} in the solution, which makes it difficult to react with each other. Therefore, no characteristic peaks of bismuth-tungsten oxides can be observed in the XRD patterns when ammonia water is not added and the pH is 1, 3 and 5. When ammonia is added, part of Bi^{3+} reacts with ammonia to form $Bi(OH)_3$. At the same time, after the H^+ in the solution is neutralized by OH^-, the mineralization ability of the remaining H^+ is not enough to make the reaction of formula (6) and formula (7) occur, so the existence of Bi_2WO_6 cannot be detected in the XRD pattern. When the pH of the solution is 7 or 9, H_2WO_4 reacts with OH^- to form WO_4^{2-}, and Bi^{3+} hydrolyzes and polymerizes to form a high polymer (formula 4) which combines with WO_4^{2-}, resulting in more Bi and less W during synthesis. As a result, $Bi_{3.84}W_{0.16}O_{6.24}$ is formed.

3.2. SEM analysis

The morphologies of the samples were measured by the SEM, as seen in Figures 3-5. Figure 3 shows the SEM micrograph of the pure BiOBr sample, which has many banded structures with a length of about 1-2 μm. Combined with the above three pictures, it can be seen that with the addition of ammonia, the stacking area of the strip structure decreases and the aggregation structure of irregular particles increases, indicating that the addition of ammonia is not conducive to the formation of regular structure.

3.3. DRS analysis

The optical properties of samples were characterized by using the DRS technique. Figure 6 shows the UV-Vis diffuse reflection spectra of the as-synthesized samples. It can be found that the maximal absorbance wavelength of pure BiOBr (no ammonia water added) is about 453 nm.

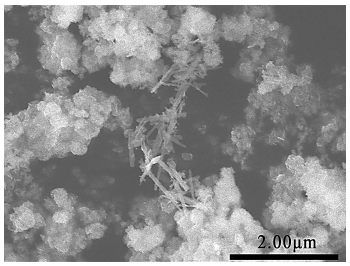

Figure 4. SEM image of the samples: adjust pH to 1 with ammonia water.

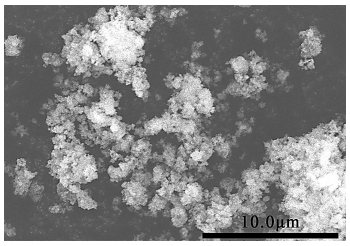

Figure 5. SEM image of the samples: adjust pH to 7 with ammonia water.

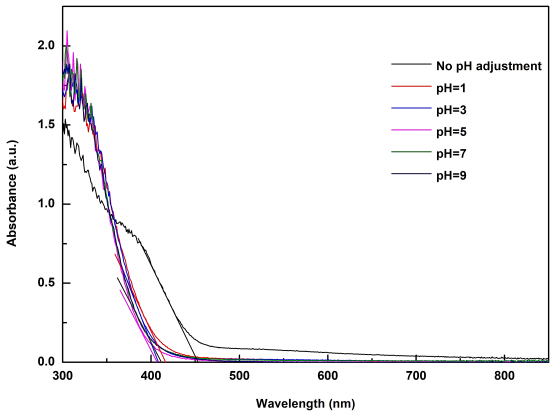

Figure 6. UV-vis diffuse reflection spectra of the as-synthesized samples.

The maximal absorbance wavelengths for pH = 1, 3, 5, 7, 9 are 416, 408, 406, 412, 412 nm, respectively. It can be seen from the spectrum that all prepared samples have light response in the visible light region. For the catalysts synthesized under different pH conditions adjusted with ammonia water, there was no significant difference in the optical absorption range. Compared with other samples, the absorption wavelength of bare BiOBr has a significant red-shift in the visible light region. According to the following formula, the band gap of the prepared photocatalyst can be obtained [11].

$$E_g = hc/\lambda_0 \approx 1240/\lambda_0 \quad (8)$$

where λ_0 and E_g represent the maximum absorption wavelength and band gap energy, respectively. The estimated values of band gap for pure BiOBr and samples synthesized at pH = 1, 3, 5, 7, 9 are 2.74, 2.98, 3.04, 3.05, 3.00, 3.00 eV, respectively.

3.4. Photocatalytic performance

3.4.1. Effect of synthetic pH

Photocatalytic degradations of the as-synthesized materials under different synthesis pH conditions (Figure 7) were comparatively evaluated by testing SDZ photodegradation under UV-visible radiation at room temperature for 2 hours. As is shown that the catalysts synthesized under different pH conditions exhibit much higher photocatalytic activity than the pure BiOBr and the BiOBr/$Bi_{3.84}W_{0.16}O_{6.24}$ (synthesized under pH = 7) shows the highest photocatalytic activity, which the degradation efficiency can reach 91%.

3.4.2. Effect of initial solution pH

Because the pH value in the actual antibiotic wastewater has a wide range of fluctuations, it is of great significance to explore the degradation efficiency of SDZ under different pH values. The initial solution pH was adjusted by 0.1 mol/L hydrochloric acid and sodium hydroxide. The influence of various initial pH for SDZ degradation was detected in Figure 8.

The results showed that the photocatalytic degradation efficiency under different pH values shows the following order: pH = 7 > pH = 9 > pH = 5 > pH = 3 > pH = 11. It can be concluded that, compared with acidic and alkaline environments, the catalyst was more conducive to the degradation of SDZ under neutral conditions. This may be attributed to the fact that in a highly acidic solution, excess H^+ competed with SDZ molecules for limited active sites on the catalyst surface, thereby reducing the photocatalytic degradation efficiency.

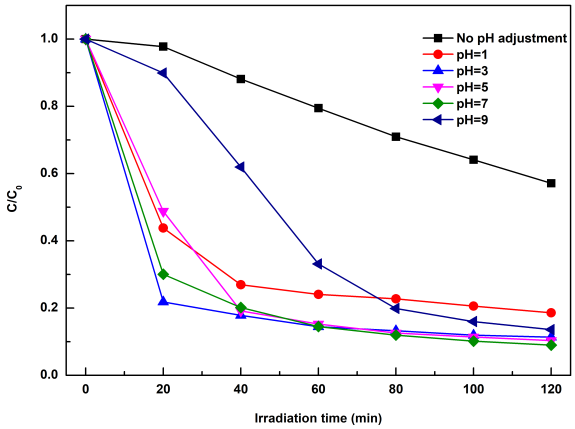

Figure 7. Photocatalytic degradation under different synthesis pH conditions.

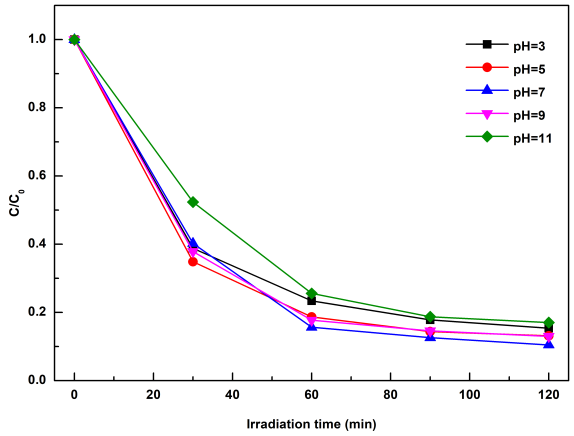

Figure 8. Photocatalytic degradation under different initial SDZ pH conditions.

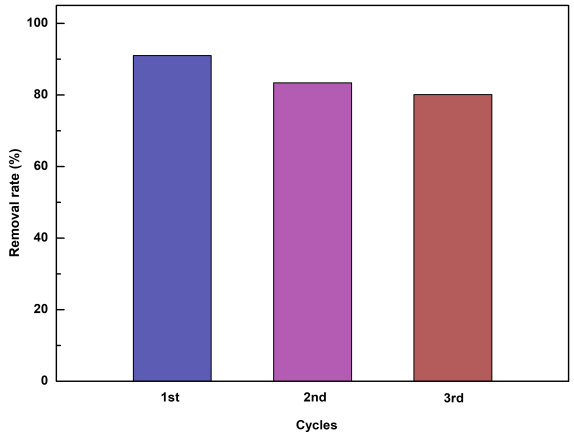

Figure 9. Recycled runs for photodegradation of SDZ.

At the same time, the degradation activity under alkaline conditions was lower than that under neutral conditions, which was due to the interaction between the hydroxyl radicals as well as the competition between the hydroxyl anion with SDZ in the absorption of the photocatalyst surface in high alkaline solution [12-14].

3.5. Stability and reusability evaluation of the catalyst

The stability of the BiOBr/$Bi_{3.84}W_{0.16}O_{6.24}$ was investigated by recycled test for photodegradation of SDZ for three cycles. As displayed in Figure 9, the removal rate of SDZ still showed excellent performance after three-cycle run. The removal rate was 80.1% after three cycles, demonstrating that the product maintained high reusability for its practical application.

3.6. The proposed mechanism

In the photocatalytic process, the main reactive species were the hydroxyl radicals (•OH), superoxide radicals ($•O_2^-$), and holes (h^+) [15,16]. To study the roles of reactive species in degradation of SDZ, the degradation experiments were conducted in the presence of scavengers.

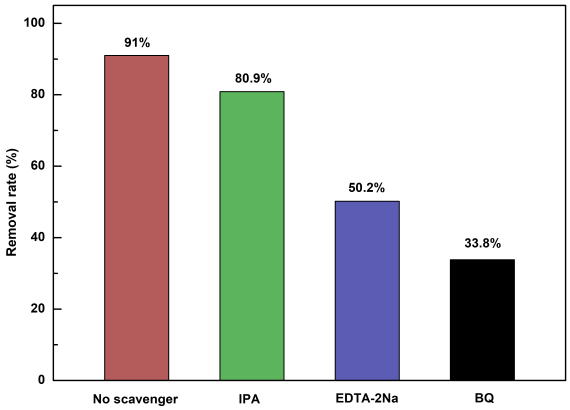

Figure 10. The effect of different radical scavengers on the degradation of SDZ.

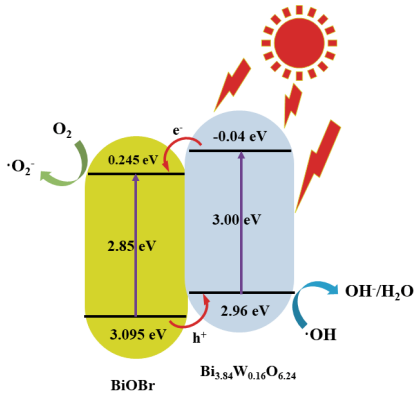

Figure 11. Photocatalytic mechanism of BiOBr/$Bi_{3.84}W_{0.16}O_{6.24}$ under the simulated sunlight irradiation.

Isopropyl alcohol (IPA), benzoquinone (BQ) and ethylenediaminetetraacetic acid disodium salt (EDTA-2Na) were added to capture •OH, $•O_2^-$ and h^+, respectively [17,18]. The experimental results were shown in Figure 10.

As depicted in Figure 10, when IPA was added to the system, the degradation efficiency was reduced by 10.1%, indicating that the effect of •OH in the degradation of SDZ was not obvious. In comparison, after adding BQ or EDTA-2Na to the system, the degradation efficiency decreased significantly and the degradation rate decreased from 91 to 33.8 and 80.9%, respectively. This result demonstrated that $•O_2^-$ and h^+ played a vital role in the degradation process.

The potentials of the CB and VB edges of BiOBr and $Bi_{3.84}W_{0.16}O_{6.24}$ were evaluated by Mulliken electronegativity theory [19,20]:

$$E_{VB}=\chi-E^e+0.5E_g \quad (9)$$

$$E_{VB}=E_{CB}+E_g \quad (10)$$

where E_{VB} is the valence band (VB) edge potential, E_{CB} is the conduction band (CB) edge potential, *X* is the absolute electronegativity of the semiconductor which is the geometric mean of the electronegativity of the constituent atoms. The χ values for BiOBr and $Bi_{3.84}W_{0.16}O_{6.24}$ are 6.17eV [21] and 5.96 eV. Eg is the band gap energy of the semiconductor and E^e is the energy of free electrons on the hydrogen scale (about 4.5 eV). Therefore, according to the equation above, it is theoretically speculated that the band edge potentials of CB and VB of the BiOBr and $Bi_{3.84}W_{0.16}O_{6.24}$ are 0.245/3.095 eV and -0.040/2.960 eV, respectively.

Combined with the above calculation results and the experimental analysis of free radical capture, we proposed a possible photocatalytic degradation mechanism, as shown in Figure 11.

Under light irradiation, BiOBr and $Bi_{3.84}W_{0.16}O_{6.24}$ were excited to generate electrons and holes. Since the valence band (VB) potential of BiOBr was more correct than that of $Bi_{3.84}W_{0.16}O_{6.24}$, the photogenerated holes in the VB of BiOBr will transfer to the VB of $Bi_{3.84}W_{0.16}O_{6.24}$. The conduction band (CB) potential of $Bi_{3.84}W_{0.16}O_{6.24}$ was more negative than that of BiOBr, so the photogenerated electrons generated in the CB of $Bi_{3.84}W_{0.16}O_{6.24}$ will transfer to the CB of BiOBr, and this effectively inhibits the recombination between photogenerated holes and electrons [22]. The CB potential of $Bi_{3.84}W_{0.16}O_{6.24}$ was less negative than $O_2/·O_2^-$ (-0.046 eV vs. NHE), indicating that photogenerated electrons cannot reduce O_2 to $·O_2^-$ [23]. However, the reactive species capture experiments confirmed that $·O_2^-$ was formed during the photocatalytic reaction. This may be due to the generation of photogenerated electrons at the top of the CB of $Bi_{3.84}W_{0.16}O_{6.24}$, which is higher than the $O_2/·O_2^-$ reduction potential [24,25]. Since the VB potential of BiOBr was higher than $H_2O/·OH$ (1.99 eV vs. NHE) and $OH^-/·OH$ (2.34 eV vs. NHE) [26], the photogenerated holes in the VB could react with H_2O and OH^- to form ·OH [27]. In addition, the stored photogenerated holes could directly oxidize the organic contaminant.

The chemical reactions that produce these active substances during the photodegradation process can be summarized as follows:

$$BiOBr/Bi_{3.84}W_{0.16}O_{6.24}+h\nu \rightarrow e^-_{CB}+h^+_{VB} \quad (11)$$

$$e^-_{CB}+O_2 \rightarrow ·O_2^- \quad (12)$$

$$h^+_{VB} + H_2O \rightarrow \cdot OH + H^+ \quad (13)$$

$$h^+_{VB} + OH^- \rightarrow \cdot OH \quad (14)$$

$$OH + h^+_{VB} + \cdot O_2^- + SDZ \rightarrow H_2O + CO_2 + \text{Degradation product} \quad (15)$$

4. Conclusions

In summary, it was found for the first time that BiOBr/$Bi_{3.84}W_{0.16}O_{6.24}$ (pH = 7) has good photocatalytic degradation performance for SDZ under UV-visible light irradiation. After 2h of light, the degradation rate could reach 91%. The effect of the initial SDZ solution pH was assessed and the result indicated that the removal rate in the neutral environment was better than that in the acidic and alkaline environment. The results obtained from the reusability of the catalyst proved that the composite material has high stability. Furthermore, radical capture experiments showed that the photocatalytic degradation of SDZ is mainly due to the oxidation of $\bullet O_2^-$ and h^+.

Disclosure statement

Conflict of interests: The authors declare that they have no conflict of interest.
Author contributions: All authors contributed equally to this work.
Ethical approval: All ethical guidelines have been adhered.
Sample availability: Samples of the compounds are available from the author.

ORCID

Zhenzhao Pei
https://orcid.org/0000-0003-4298-7539
Feng Li
https://orcid.org/0000-0002-6106-3350

References

[1]. Liu, X.; Steele, J. C.; Meng, X.-Z. *Environ. Pollut.* **2017**, *223*, 161–169.
[2]. Haller, M. Y.; Müller, S. R.; McArdell, C. S.; Alder, A. C.; Suter, M. J.-F. *J. Chromatogr. A* **2002**, *952* (1–2), 111–120.
[3]. Li, Y.; Liu, X.; Zhang, B.; Zhao, Q.; Ning, P.; Tian, S. *Environ. Sci. Process. Impacts* **2018**, *20* (3), 513–522.
[4]. Hedgespeth, M. L.; Sapozhnikova, Y.; Pennington, P.; Clum, A.; Fairey, A.; Wirth, E. *Sci. Total Environ.* **2012**, *437*, 1–9.
[5]. Guo, F.; Shi, W.; Li, M.; Shi, Y.; Wen, H. *Sep. Purif. Technol.* **2019**, *210*, 608–615.
[6]. Sivakumar, A.; Murugesan, B.; Loganathan, A.; Sivakumar, P. *J. Taiwan Inst. Chem. Eng.* **2014**, *45* (5), 2300–2306.
[7]. Meng, X.; Zhang, Z. *J. Mol. Catal. A Chem.* **2016**, *423*, 533–549.
[8]. Wang, C.; Zhu, L.; Song, C.; Shan, G.; Chen, P. *Appl. Catal. B* **2011**, *105* (1–2), 229–236.
[9]. Hou, L.; Hua, H.; Gan, L.; Liu, Y.; Yuan, C.; Liu, S. *J. Nanopart. Res.* **2015**, *17* (4), 185.
[10]. Li, X.; Wang, L.; Xu, D.; Lin, J.; Li, P.; Lin, S.; Shi, W. *CrystEngComm* **2015**, *17* (11), 2421–2428.
[11]. Linsebigler, A. L.; Lu, G.; Yates, J. T., Jr. *Chem. Rev.* **1995**, *95* (3), 735–758.
[12]. Kasiri, M. B.; Aleboyeh, H.; Aleboyeh, A. *Appl. Catal. B* **2008**, *84* (1–2), 9–15.
[13]. Nezamzadeh-Ejhieh, A.; Khorsandi, S. *J. Ind. Eng. Chem.* **2014**, *20* (3), 937–946.
[14]. Parvaz, S.; Rabbani, M.; Rahimi, R. *Mater. Sci. Eng. B Solid State Mater. Adv. Technol.* **2021**, *263* (114863), 114863.
[15]. Wang, F.; Gu, Y.; Yang, Z.; Xie, Y.; Zhang, J.; Shang, X.; Zhao, H.; Zhang, Z.; Wang, X. *Appl. Catal. A Gen.* **2018**, *567*, 65–72.
[16]. Liu, J.; Li, H.; Du, N.; Song, S.; Hou, W. *RSC Adv.* **2014**, *4* (59), 31393–31399.
[17]. An, W.; Tian, L.; Hu, J.; Liu, L.; Cui, W.; Liang, Y. *Appl. Surf. Sci.* **2020**, *534* (147518), 147518.
[18]. Xia, J.; Di, J.; Yin, S.; Xu, H.; Zhang, J.; Xu, Y.; Xu, L.; Li, H.; Ji, M. *RSC Adv.* **2014**, *4* (1), 82–90.
[19]. Yu, J.; Xiong, J.; Cheng, B.; Yu, Y.; Wang, J. *J. Solid State Chem.* **2005**, *178* (6), 1968–1972.
[20]. Liu, Z.; Ran, H.; Niu, J.; Feng, P.; Zhu, Y. *J. Colloid Interface Sci.* **2014**, *431*, 187–193.
[21]. An, W.; Cui, W.; Liang, Y.; Hu, J.; Liu, L. *Appl. Surf. Sci.* **2015**, *351*, 1131–1139.
[22]. Zhang, S.; Yang, J. *Ind. Eng. Chem. Res.* **2015**, *54* (41), 9913–9919.
[23]. Yang, L.; Liang, L.; Wang, L.; Zhu, J.; Gao, S.; Xia, X. *Appl. Surf. Sci.* **2019**, *473*, 527–539.
[24]. Ye, L.; Chen, J.; Tian, L.; Liu, J.; Peng, T.; Deng, K.; Zan, L. *Appl. Catal. B* **2013**, *130–131*, 1–7.
[25]. Ye, L.; Liu, J.; Jiang, Z.; Peng, T.; Zan, L. *Appl. Catal. B* **2013**, *142–143*, 1–7.
[26]. Jiang, Z.; Wan, W.; Li, H.; Yuan, S.; Zhao, H.; Wong, P. K. *Adv. Mater.* **2018**, *30* (10), 1706108.
[27]. Dong, S.; Lee, G. J.; Zhou, R.; Wu, J. J. *Sep. Purif. Technol.* **2020**, *250* (117202), 117202.